Applied Catalysis B: Environmental 162 (2015) 401–411

Contents lists available at ScienceDirect

Applied Catalysis B: Environmental

journal homepage: www.elsevier.com/locate/apcatb

# Sorption enhanced aqueous phase reforming of glycerol for hydrogen production over Pt-Ni supported on multi-walled carbon nanotubes

Chao He[a,b], Jianwei Zheng[c,d], Ke Wang[a,e], Haiqiang Lin[c,d], Jing-Yuan Wang[a,b,*], Yanhui Yang[c,d,**]

[a] Residues and Resource Reclamation Centre, Nanyang Environment and Water Research Institute, Nanyang Technological University, 1 Cleantech Loop, Singapore 637141, Singapore
[b] Division of Environmental and Water Resources Engineering, School of Civil and Environmental Engineering, Nanyang Technological University, 50 Nanyang Avenue, Singapore 639798, Singapore
[c] Department of Chemistry, College of Chemistry and Chemical Engineering, State Key Laboratory of Physical Chemistry for Solid Surface, National Engineering Laboratory for Green Chemical Productions of Alcohols, Ethers and Esters, Xiamen University, Xiamen 361005, China
[d] School of Chemical and Biomedical Engineering, Nanyang Technological University, 50 Nanyang Avenue, Singapore 639798, Singapore
[e] School of Municipal and Environmental Engineering, Harbin Institute of Technology, 73 Huanghe Road, Harbin, Heilongjiang 150090, China

ARTICLE INFO

*Article history:*
Received 17 March 2014
Received in revised form 28 June 2014
Accepted 4 July 2014
Available online 11 July 2014

*Keywords:*
Bimetallic catalyst
Platinum-nickel
Platinum-palladium
Water-gas shift
$CO_2$ removal

ABSTRACT

In this study, multi-walled carbon nanotubes supported Pt and Pt-based bimetallic catalysts were prepared and their catalytic activities were investigated to screen effective and economical catalyst for $H_2$ production in catalytic aqueous phase reforming (CAPR) of glycerol. Nickel promoted Pt catalyst with optimized Ni:Pt molar ratio afforded highest glycerol conversion rate (81.21%) and carbon conversion to gas (15.3%) although hydrogen gasification ratio (7.2%) was poorer than that of noble metals promoted Pt-based bimetallic catalysts. Adding CaO significantly enhanced the fraction and selectivity of $H_2$ over Pt-Ni catalyst and those of $CH_4$ were reduced to a negligible level, which was possibly attributed to the facilitated water-gas shift reaction and inhibited methanation through in-situ $CO_2$ sorption via carbonation. Results suggested that Pt-Ni bimetallic catalysts improved dehydrogenation–decarboxylation and dehydration–hydrogenation reactions, leading to high glycerol conversions. Introducing CaO further favored C–C bond cleavage towards high $H_2$ yield. The catalytic performance can be completely recovered after regenerating the catalyst and adding sacrificial CaO. In terms of reduced consumption of precious metal catalyst, excellent catalyst performance and hydrothermal stability, combination of Pt-Ni bimetallic catalyst and CaO additive was identified as an effective catalytic system for $H_2$ production in CAPR of glycerol.



## 1. Introduction

Biomass derived alternative energy carriers and chemicals are becoming increasingly important due to rapid depletion of fossil fuel and associated environmental problems. Biodiesel produced from non-food feedstocks (e.g. lignocellulosic biomass and microalgae) is regarded as a promising alternative biofuel [1]. However, approximate 10 wt.% of glycerol by-product is generated during the biodiesel processing [2]. The ever increasing biodiesel production leads to excess glycerol in market, which attracts great attention to increase overall benefits during biodiesel production by re-utilizing this main by-product [3]. Unlike applications of pure glycerol in cosmetics, pharmaceuticals and chemicals, re-utilization of crude glycerol is limited by its high water content [4].

Direct conversion of glycerol to hydrogen rich gas via thermochemical processes has been extensively explored [5]. Catalytic aqueous phase reforming (CAPR) is one of the technically feasible approaches to produce hydrogen with trace amounts of CO from oxygenated hydrocarbons derived from biomass under hydrothermal conditions of 175–265 °C [6] and 15–50 bar [7]. The CAPR reaction mainly includes dehydrogenation (C–C bond cleavage) and

* Corresponding author at: Residues and Resource Reclamation Centre, Nanyang Environment and Water Research Institute, Nanyang Technological University, 1 Cleantech Loop, Singapore 637141, Singapore. Tel.: +65 6790 4100; fax: +65 6792 7319.
** Corresponding author at: School of Chemical and Biomedical Engineering, Nanyang Technological University, 50 Nanyang Avenue, Singapore 639798, Singapore. Tel.: +65 6316 8940; fax: +65 6794 7553.
*E-mail addresses:* jywang@ntu.edu.sg (J.-Y. Wang), yhyang@ntu.edu.sg (Y. Yang).

http://dx.doi.org/10.1016/j.apcatb.2014.07.012
0926-3373/

water-gas shift (WGS) reaction of adsorbed CO [8]. CAPR of glycerol to $H_2$ involves the following reactions [9,10].

$$C_3H_8O_3 + 3H_2O \rightarrow 3CO_2 + 7H_2 \quad (1)$$

WGS reaction:

$$CO + H_2O \leftrightharpoons CO_2 + H_2 \quad (2)$$

Methanation reactions [4]:

$$CO + 3H_2 \rightarrow CH_4 + H_2O \quad (3)$$

$$CO_2 + 4H_2 \rightarrow CH_4 + 2H_2O \quad (4)$$

Therefore, desired catalysts in CAPR process should be highly active in C–C bond cleavage and WGS reaction while C–O bond cleavage and methanation reactions should be inhibited.

Platinum supported on alumina ($Pt/Al_2O_3$) has been reported as active and selective catalyst in CAPR [11–13]. To increase $H_2$ production and selectivity, intensive studies on CAPR of glycerol (including other polyols, such as ethylene glycol) for $H_2$ production over Pt-based bimetallic catalysts have also been conducted, such as Pt-Re [14–16], Pt-Co [17,18], and Pt-Ni bimetallic catalysts [4–6,10,18–20]. Alloying Pt with Re showed improved C–C bond cleavage and glycerol conversion with relatively poor $H_2$ selectivity [14–16]. Pt-Co bimetallic catalyst reported by Wang et al. [17] achieved a high $H_2$ production rate of 4.6 mmol g $cat^{-1}$ $min^{-1}$ from CAPR of ethylene glycol. Similarly, Pt-Ni exhibited higher $H_2$ and less alkane formation from CAPR of glycerol than Pt monometallic catalyst [19]. More importantly, adding base metals (i.e. Co and Ni) into Pt catalyst can significantly reduce the usage of noble metals [17].

Apart from Pt-based catalysts, taken into account of good activity of Ni for C–C bond cleavage and that of Cu in WGS reaction, 60% of glycerol was converted at 270 °C with high $H_2$ selectivity and suppressed methanation over a Ni-Cu catalyst [21]. Byrd et al. [2] reported that glycerol with concentration up to 40 wt.% can be completely gasified to produce near-theoretical $H_2$ yield in the presence of $Ru/Al_2O_3$ in supercritical water (SCW). Nonetheless, high $CH_4$ yield reduced $H_2$ purity.

Catalyst stability in CAPR is another challenging issue [22]. Due to the phase transformation of $\gamma$-$Al_2O_3$ to boehmite [AlO(OH)], $Pt/\gamma$-$Al_2O_3$ was not stable even under mild hydrothermal condition [13,22]. Besides, CAPR is a structure sensitive reaction [23]. Compared to platinum nanoparticle size, structural properties and support nature exhibited more remarkable effects on catalytic performance. Through catalytic performance screening of Pt-based catalysts supported on various oxides (i.e. $Al_2O_3$, $ZrO_2$, $CeO_2$, and MgO) in CAPR of glycerol, Menezes et al. [24] found that MgO demonstrated the best activity for $H_2$ production with low alkanes as a result of the basic nature of MgO. Due to unique properties (e.g. thermal resistance, metal dispersion, acid–base and redox properties, activity in WGS reaction, inhibition of coking and methanation) of $CeO_2$, $CeO_2$-doped $Al_2O_3$ was employed as support materials for Pt catalyst to enhance $H_2$ selectivity and carbon conversion to gas with low $CH_4$ yield [25].

Due to the diffusion limitation induced by irregular porous structure of activated carbon, gaseous products cannot be removed rapidly and thus hydrogen production was inhibited [26]. Kim et al. [26] claimed that ordered mesoporous carbon was an effective carbonaceous support due to its hydrothermal stability and open mesoporous structure. The activity of supported Pt-Re catalyst followed the order of CMK-3 > activated carbon > $SiO_2$ > $Al_2O_3$ [27]. Carbon nanotubes (CNTs), both single-walled carbon nanotubes (SWNTs) and multi-walled carbon nanotubes (MWCNTs), have been reported to be superior catalyst support materials for hydrothermal gasification [17,28], even under SCW conditions [29].

In addition to catalyst design, some novel processes have also been developed in order to enhance $H_2$ yield and selectivity. For instance, dolomite was conventionally selected as $CO_2$ absorber to enhance catalytic steam gasification process towards more $H_2$ yield with high purity via in-situ $CO_2$ removal and carbonation [30]. More recently, calcium oxide has been employed to achieve high $H_2$ and $CH_4$ selectivity in supercritical water gasification of biomass [31]. The WGS reaction is regarded as the rate-limiting step in CAPR reaction network of glycerol over Pt-based catalysts [9]. Rapid $CO_2$ removal would be able to shift WGS reaction towards selective $H_2$ production. Along this line, MWCNTs supported Pt monometallic and Pt-based bimetallic catalysts were prepared for $H_2$ production in CAPR of glycerol in this study. Moreover, CaO was selected as the in-situ $CO_2$ absorber. The effects of alloying the second metal with Pt and introducing CaO as $CO_2$ acceptor on gas and liquid products yields were discussed in detail. Based on the reaction results, reaction pathways in present CAPR of glycerol were proposed.

## 2. Experimental

### 2.1. Materials

Chloroplatinic acid hexahydrate ($H_2PtCl_6{\cdot}6H_2O$, >37.5% Pt basis), palladium chloride ($PdCl_2$, ReagentPlus, 99%), ruthenium (III) nitrosyl nitrate solution ($HN_4O_{10}Ru$,), nickel (II) nitrate hexahydrate ($Ni(NO_3)_2{\cdot}6H_2O$, 99.999%), copper (II) nitrate hydrate ($Cu(NO_3)_2{\cdot}xH_2O$, 99.999%), concentrated nitric acid ($HNO_3$, ACS reagent, 69%), glycerol (≥99.5%), 1,2-propanediol (ACS reagent, ≥99.5%), calcium hydroxide ($Ca(OH)_2$, Reag. Ph. Eur., ≥96%), calcium carbonate ($CaCO_3$, ReagentPlus) and calcium oxide (CaO, reagent grade) were purchased from Sigma–Aldrich. Hydroxyacetone (95%) and cobalt (II) chloride (Anhydrous, 97%) were provided by Alfa Aesar. All these chemicals were used without further purification. Deionized (DI) water produced from Millipore Milli-Q water purification system was used throughout entire experiments.

### 2.2. Catalyst preparation

MWCNTs (Shenzhen Nanotech Port Co., China) were employed as support materials during monometallic and bimetallic catalysts preparation. The pristine MWCNTs were refluxed in concentrated nitric acid at 120 °C for 4 h under stirring to remove metallic impurities and introduce oxygen-containing functional groups onto the surface of MWCNTs, thereby facilitating uniform precipitation of metal precursors [32]. The functionalized MWCNTs were washed and prepared following the procedure described by Nassr et al. [33], which were denoted as FCNTs thereafter.

Both monometallic and bimetallic platinum catalysts were prepared by incipient wetness impregnation method. Specifically, a 5 wt.% Pt supported on FCNTs catalyst was prepared by impregnating 100 mg of FCNTs with 722 μL of 20 mg/mL $H_2PtCl_6{\cdot}6H_2O$ solution and 30 mL DI water in a 50 mL round bottomed flask. The mixture was vigorously stirred by magnetic stirring bar at 650 rpm for 2 h at room temperature. The slurry was dried by rotary evaporator at 60 °C under 200 mbar. The Pt-FCNTs composite was further oven dried at 100 °C for 12 h. The prepared catalyst composite was pulverized into fine powders in agate mortar and reduced at 350 °C for 2 h under a $H_2$ flow rate of 40 mL/min. The as-synthesized catalyst with 5 wt.% Pt loading was denoted as 5Pt/CNT.

Similarly, bimetallic platinum catalysts were prepared in the presence of Pt and transition metal precursors at a fixed Pt loading of 5 wt.% and Pt to promoter atomic ratio of 1:1 following the same procedure. These catalysts were denoted as 5Pt1.5Ni/CNT, 5Pt1.5Co/CNT, 5Pt1.6Cu/CNT, 5Pt2.7Pd/CNT, and 5Pt2.6Ru/CNT. For comparison, another two Pt to Ni atomic ratios (2:1) and (1:2) were

**Table 1**
Chemical composition and physical characteristics of as-synthesized catalysts.

| Sample | Metal type and loading (wt.%)[a] | $S_{BET}$ ($m^2$/g) | Total pore volume ($cm^3$/g) | Average pore diameter (nm) | $H_2$ uptake (μmol/g cat) | CO uptake (μmol/g cat) |
|---|---|---|---|---|---|---|
| FCNTs | – | 164.6 | 1.68 | 40.8 | – | – |
| 5Pt/CNT | 4.88 (Pt) | 174.7 | 1.64 | 37.5 | 23.37 | 37.95 |
| 5Pt0.75Ni/CNT | 4.70 (Pt), 0.74 (Ni) | 158.6 | 1.00 | 25.3 | 27.85 | 44.52 |
| 5Pt1.5Ni/CNT | 4.67 (Pt), 1.36 (Ni) | 140.6 | 1.29 | 36.7 | 32.11 | 45.91 |
| 5Pt3Ni/CNT | 4.65 (Pt), 2.75 (Ni) | 153.6 | 0.80 | 20.9 | 20.80 | 34.00 |
| 5Pt1.5Co/CNT | 4.74 (Pt), 1.33 (Co) | 141.1 | 1.03 | 29.1 | – | – |
| 5Pt1.6Cu/CNT | 4.61 (Pt), 1.57 (Cu) | 136.7 | 1.19 | 34.9 | – | – |
| 5Pt2.7Pd/CNT | 4.76 (Pt), 2.45 (Pd) | 155.0 | 1.12 | 29.0 | – | – |
| 5Pt2.6Ru/CNT | 4.68 (Pt), 2.23 (Ru) | 139.5 | 1.22 | 35.1 | – | – |

[a] Determined by ICP-OES.

attempted, resulting in a final Ni loading of 0.75 wt.% and 3.0 wt.%, respectively. These two catalysts were denoted as 5Pt0.75Ni/CNT and 5Pt3Ni/CNT accordingly. To determine actual metal loadings, the catalysts were digested in concentrated Aqua Regia in High Performance Microwave Digestion System (Milestone Inc.) under 200 °C for 30 min and diluted into 100 mL solution after cooling down. The dissolved metals were analyzed using PerkinElmer Optima 8300 inductively coupled plasma optical emission spectrometer (ICP-OES). The determined metal loadings were close to the theoretical values. The chemical composition and physicochemical characteristics of all these catalysts are described in Table 1.

### 2.3. Catalyst characterization

Textural characteristics of as-synthesized catalysts were measured by Quantachrome Autosorb sorption system. Prior to liquid nitrogen adsorption–desorption at −196 °C, the catalysts were degassed at 150 °C for 12 h under vacuum. Specific surface areas of catalysts were determined through multi-point Brunauer–Emmett–Teller (BET) method. Pore volume and average pore diameter were calculated using Barrett–Joyner–Halender (BJH) method based on $N_2$ desorption data.

Chemisorption uptakes of $H_2$ and CO on catalysts were conducted on Micromeritics ASAP 2020 (M + C) analyzer using static volumetric method following a modified procedure described elsewhere [34]. Briefly, ca. 500 mg of as-synthesized catalyst was reduced in high-purity $H_2$ at 350 °C for 4 h and then evacuated for 1 h to ensure complete removal of chemisorbed species. An initial isotherm was measured under 100–600 Torr at 35 °C. Subsequently, evacuation was carried out for 30 min at 35 °C to remove reversibly adsorbed adsorbates ($H_2$ and CO) on catalyst surface prior to measurement of a repetitive isotherm under the same condition. Finally, the uptakes of irreversibly chemisorbed adsorbates on catalysts were derived by the difference between the initial and repetitive isotherms.

X-ray diffraction (XRD) patterns of catalysts were determined over a $2\theta$ range from 10° to 80° using Philips PANAlytical X'pert Pro powder X-ray diffractometer equipped with a graphite monochromator using Cu-Kα radiation X-ray source operated at 40 kV and 30 mA. High resolution transmission electron microscopy (HRTEM) images were taken on Philips Analytical FEI Tecnai F30 electron microscope operated at an acceleration voltage of 300 kV. The catalysts were sonicated in ethanol for 5 min, deposited onto carbon coated copper grids and then dried before analysis.

### 2.4. Catalyst testing

The CAPR of glycerol was carried out in a 50 mL stainless steel micro bench reactor (Parr 4592 model) equipped with magnetic drive stirrer, PTFE liner, and PID controller (Parr Instrument Co., USA). The dead volume of the autoclave with PTFE liner was calibrated as 43 mL by GilAir Plus air pump. Typically, 15 mL of 10 wt.% glycerol stock solution, 100 mg catalysts, and a specific amount of CaO were loaded into the PTFE vessel. The reactor was purged with nitrogen gas for 5 min and pressurized to an initial $N_2$ pressure of 30 bar, which served as an internal standard for final gas yield calculation. Subsequently, the reactor was heated to 230 °C using an external electric heating mantle under a stirring speed of 500 rpm. After maintaining at 230 °C for 4 h, the reactor was quenched to room temperature in ice water bath rapidly. Gaseous products were gently released to Tedlar gas bags through the gas outlet valve. After depressurization, the reactor was opened for liquid products sampling and spent catalysts recovery. The liquid products were collected and filtered through 0.45 μm PTFE membrane filters for further analysis. The spent catalysts were washed with DI water and oven dried at 100 °C overnight.

### 2.5. Products analyses

#### 2.5.1. Gas products

Gaseous products were analyzed using gas chromatograph (Agilent Technologies 7890A, USA) equipped with dual thermal conductivity detectors (GC-TCD/TCD) with HayeSep Q, HayeSep C, HayeSep R, Molesieve 13X, and Molesieve 5A columns for gas separation. Hydrogen, carbon dioxide, methane, and nitrogen were detected in gaseous products.

#### 2.5.2. Liquid products

A 10 μL liquid solution was injected into an UltiMate 3000 high performance liquid chromatography (HPLC) equipped with an UV–vis detector for analysis. Liquid analytes separation was carried out by Bio-Rad Aminex HPX-87H ion exclusion column (300 mm × 7.8 mm) with a 5 mM $H_2SO_4$ aqueous solution as the mobile phase at a flow rate of 0.7 mL/min and column temperature of 33 °C. The dissolved calcium ion concentration in liquid products was determined by ICP-OES.

### 2.6. Catalyst regeneration and recycle experiments

Thermogravimetric analysis (TGA) was performed by STA 449 F3 Jupiter Simultaneous TG–DTA/DSC Apparatus (NETZSCH-Gerätebau GmbH) under $N_2$ atmosphere with a fixed flow rate of 20 mL/min. The weight loss (TG) and the weight loss rate (DTG) of catalysts and standard chemicals were recorded dynamically from 50 to 900 °C at a heating rate of 10 °C/min. TGA of 5Pt1.5Ni/CNT + 180 mg CaO after first catalytic run was conducted to determine the peak temperature of spent catalyst with pure $CaCO_3$ and $Ca(OH)_2$ as standard chemicals. Subsequently, the spent catalysts were calcined at the peak temperature determined by TGA under 40 mL/min of $N_2$ for 1 h. The calcined catalysts were reused with 180 mg fresh CaO powders in the next catalytic reaction experiment.

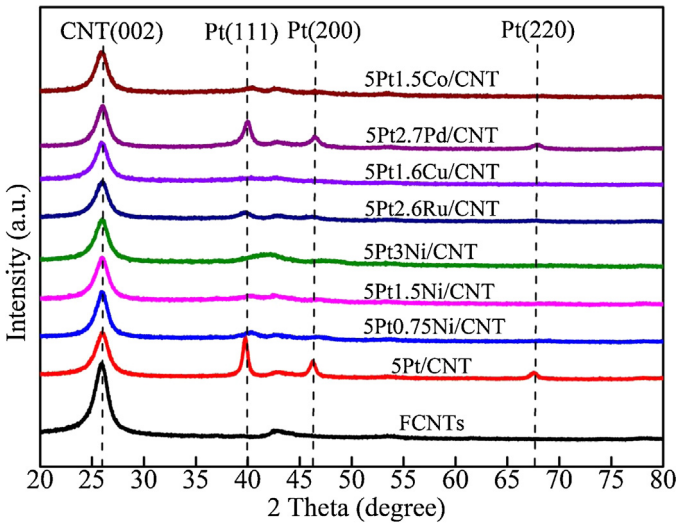


**Fig. 1.** X-ray diffraction patterns of FCNTs and as-synthesized catalysts supported on FCNTs.

### 2.7. Terms and definitions for catalysts activity and selectivity evaluation

The catalysts were evaluated in terms of glycerol conversion rate, carbon conversion to gas, hydrogen gasification ratio, $H_2$ yield, $H_2$ selectivity, and $CH_4$ selectivity according to following equations proposed previously [15].

$$\text{Glycerol conversion rate (\%)} = \left(1 - \frac{\text{Moles of glycerol remaining in liquid phase}}{\text{Moles of glycerol in feedstock}}\right) \times 100$$

$$\text{Carbon conversion to gas (\%)} = \frac{\text{C atoms in gas products}}{\text{Total C atoms in feedstock}} \times 100$$

$$\text{Hydrogen gasification ratio (\%)} = \frac{\text{H atoms in gas products}}{\text{Total H atoms in feedstock}} \times 100$$

$$H_2\ \text{yield (mmol/g Glycerol)} = \frac{\text{Molecules of produced } H_2\ \text{(mmol)}}{\text{Mass of glycerol in feedstock (g)}}$$

$$H_2\ \text{selectivity (\%)} = \frac{\text{Molecules of produced } H_2}{\text{C atoms in gas products}} \times \frac{1}{n} \times 100$$

where $n = 7/3$, which is the $H_2/CO_2$ stoichiometric reforming ratio in Eq. (1).

$$CH_4\ \text{selectivity(\%)} = \frac{\text{C atoms in produced } CH_4}{\text{Total C atoms in gas products}} \times 100$$

## 3. Results and discussion

### 3.1. Structural and physicochemical properties of catalysts

Fig. 1 depicts XRD patterns of FCNTs and all the as-synthesized catalysts. The sharp diffraction (0 0 2) of hexagonal graphite at $2\theta$ of 25.8° that represents graphite structure of carbon nanotubes was retained after $HNO_3$ oxidation, Pt monometallic and bimetallic impregnation and reduction at high temperature [32]. The catalytic activity in CAPR reaction was reported to associate with metal nanoparticle size and dispersion on carbonaceous support [26]. As presented in Fig. 1, 5Pt/CNT displayed noticeable diffraction peaks at $2\theta$ of 39.9°, 46.1°, and weak signal at 67.4°, which were assigned to (1 1 1), (2 0 0) and (2 2 0) facets of Pt fcc structure, respectively [33]. After adding promoters, the characteristic diffraction peaks of Pt became less intensive, indicating the smaller metal nanoparticles after alloying with the second metal. Due to the low metal loadings of promoters, good dispersion as well as small particle size, the crystalline structures of promoters cannot be clearly identified in Fig. 1 as a result of XRD instrument detection limit [19].

Particle size distribution histograms of 5Pt/CNT and 5Pt1.5Ni/CNT and corresponding HRTEM images are shown in Fig. 2. Particle size distribution histograms were derived by counting 308 and 403 particles for 5Pt/CNT and 5Pt1.5Ni/CNT, resulting in an average particle size of 2.2 and 1.2 nm, respectively. After adding 1.5 wt.% of Ni, 5Pt1.5Ni/CNT presented a slightly narrower particle size distribution than 5Pt/CNT. According to the inset TEM images in Fig. 2A and B, the well dispersed Pt and Pt-Ni nanoparticles on FCNTs and the small average particle size of 1.2 nm for 5Pt1.5Ni/CNT coincided with the weak diffraction peaks in abovementioned XRD patterns. Apart from Pt-Ni alloy in Fig. 2D, Pt nanoparticles were observed elsewhere, which was in agreement with results found by de Vlieger et al. [19]. Recently, the Pt-Ni alloy structure has been presumed to be formed by a Pt-rich alloy shell with a Ni-rich core near support surface resulting from negatively charged FCNTs during catalyst preparation [33]. The presence of Pt-Ni alloy may modify the electronic environment of Pt, thereby increasing binding energy of $Pt4d_{5/2}$ and thus the Pt dispersion [10]. This claim was consistent with observations in XRD patterns.

The diffraction peaks of Pt for 5Pt2.6Ru/CNT and 5Pt2.7Pd/CNT were stronger than base metal promoted Pt bimetallic catalysts, which may be ascribed to higher metal loadings of noble metal promoters at a fixed atomic ratio of 1:1. Besides, the Pt (1 1 1) diffraction peaks for Pt-Ni catalysts slightly shifted to higher $2\theta$ values, implying that smaller Ni atoms may be incorporated into Pt fcc lattice to form Pt-Ni alloy structure [33]. The alloy formation can be further evidenced by measuring the lattice spacing on HRTEM images [35]. The lattice spacing of Pt (1 1 1) plane in 5Pt/CNT was 0.225 nm (Fig. 2C) whereas that of well resolved (1 1 1) planes in 5Pt1.5Ni/CNT was found to be 0.220 nm (Fig. 2D). The Pt-Ni alloying was more pronounced for higher Ni loading 5Pt3Ni/CNT (Pt to Ni atomic ratio of 1:2) with board peak at $2\theta$ of 41.8°. 5Pt1.5Co/CNT showed similar Pt (1 1 1) diffraction peak compared to 5Pt1.5Ni/CNT, implying the formation of Pt-Co alloying as well. Huber et al. [18] reported previously that bulk Pt-Ni or Pt-Co alloy is inclined to be formed when stoichiometric amounts of Ni or Co are introduced into Pt catalyst.

Table 1 summaries the physicochemical properties of FCNTs support material and as-synthesized catalysts. The BET specific surface area ($S_{BET}$) of FCNTs was 164.6 $m^2/g$, which was remarkably lower than that of CMK-3 (884 $m^2/g$) [26]. After impregnation of Pt, due to the formation of Pt nanoparticles on FCNTs surface, $S_{BET}$ of 5Pt/CNT slightly increased to 174.7 $m^2/g$ while average pore diameter decreased from 40.8 to 37.5 nm and total pore volume remained similar (around 1.65 $cm^3/g$). Compared with 5Pt/CNT, $S_{BET}$ (140–160 $m^2/g$), average pore diameter (0.8-1.3 $cm^3/g$), and total pore volume (20-37 nm) of Pt-based bimetallic catalysts all decreased. These physicochemical properties may contribute to different catalytic activities of these catalysts in the following discussion.

### 3.2. Catalyst screening experiments

#### 3.2.1. Hydrogen gasification ratio, carbon conversion to gas, and glycerol conversion rate

Eight catalysts were attempted in CAPR of glycerol under experimental conditions shown in Table 2. Although the initial pressure was 30 bar, the pressure increased and differed slightly when the temperature reached 230 °C, which was around 55 bar. After 4 h

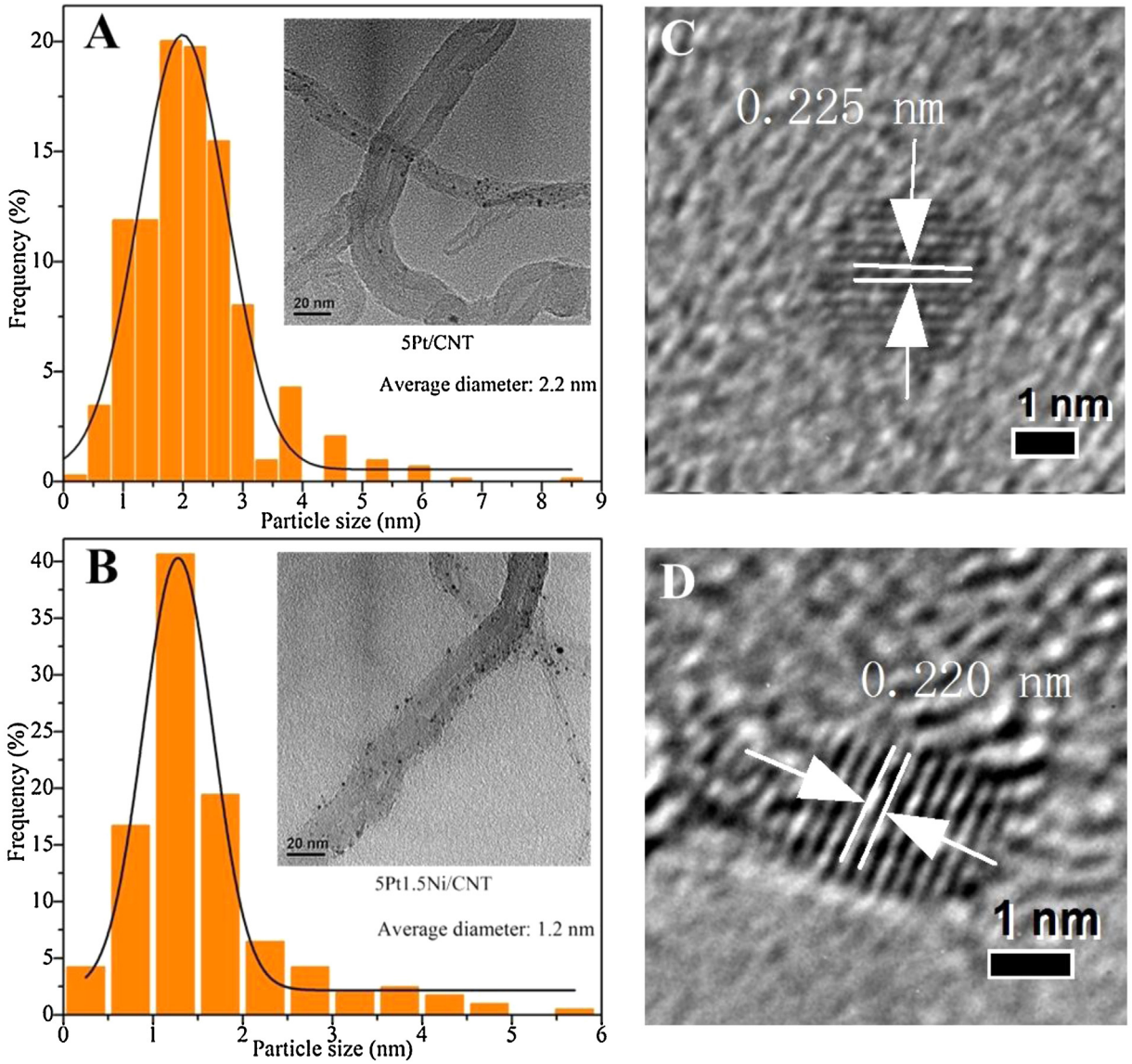


**Fig. 2.** Particle size distribution histograms of (A) 5Pt/CNT (inset: TEM image of 5Pt/CNT) and (B) 5Pt1.5Ni/CNT (inset: TEM image of 5Pt1.5Ni/CNT); HRTEM images of (C) 5Pt/CNT and (D) 5Pt1.5Ni/CNT (Arrows indicated the lattice spacing of Pt (1 1 1) plane and Pt-Ni bimetallic cluster).

of reaction, final pressure increased to different extent due to different activities of catalysts and gas production. Fig. 3 presents activities of various catalysts in terms of glycerol conversion rate, hydrogen gasification ratio, and carbon conversion to gas. Overall, adding promoters, such as Ni, Co, and Ru, improved the glycerol conversion rate except Cu and Pd. The glycerol conversion rate over 5Pt1.6Cu/CNT was only 13.5% and hydrogen gasification ratio as well as carbon conversion to gas was less than 5%. Ni and Co

**Table 2**
Experimental conditions of catalytic aqueous phase reforming of glycerol for hydrogen production.

| Catalyst | Experimental conditions | | | | |
|---|---|---|---|---|---|
| | Catalyst weight (g) | Temperature (°C) | Initial pressure (bar) | Running pressure at 230 °C (bar) | Time (h) |
| 5Pt/CNT | 0.1 | 230 | 30 | 56[a]/62[b] | 4 |
| 5Pt0.75Ni/CNT | 0.1 | 230 | 30 | 54/64 | 4 |
| 5Pt1.5Ni/CNT | 0.1 | 230 | 30 | 58/66 | 4 |
| 5Pt1.5Ni/CNT + 90 mg CaO | 0.1 | 230 | 30 | 61/67 | 4 |
| 5Pt1.5Ni/CNT + 180 mg CaO | 0.1 | 230 | 30 | 62/68 | 4 |
| 5Pt3Ni/CNT | 0.1 | 230 | 30 | 57/63 | 4 |
| 5Pt1.5Co/CNT | 0.1 | 230 | 30 | 54/64 | 4 |
| 5Pt1.6Cu/CNT | 0.1 | 230 | 30 | 54/58 | 4 |
| 5Pt2.7Pd/CNT | 0.1 | 230 | 30 | 55/69 | 4 |
| 5Pt2.6Ru/CNT | 0.1 | 230 | 30 | 57/69 | 4 |

[a] Pressure when reaction temperature reached 230 °C.
[b] Pressure after 4 h of reaction.

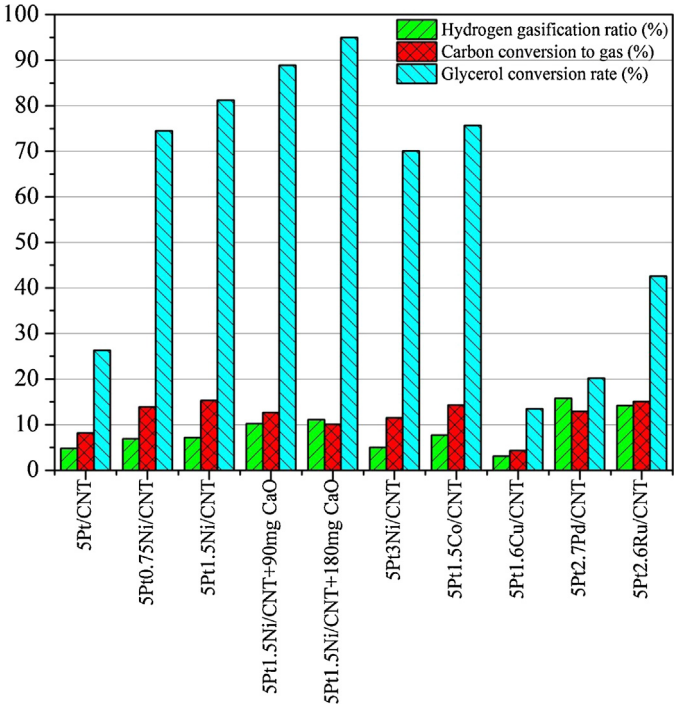


**Fig. 3.** Effects of different metal promoters and CaO amounts on glycerol conversion rate, hydrogen gasification ratio, and carbon conversion to gas during catalytic aqueous phase reforming. Operating conditions: 230 °C, an initial $N_2$ pressure of 30 bar, 15 mL of 10 wt.% glycerol with 100 mg catalyst for 4 h reaction time.

significantly enhanced the glycerol conversion rate from 26.33% for 5Pt/CNT to 81.21% and 75.67% for 5Pt1.5Ni/CNT and 5Pt1.5Co/CNT, respectively. The carbon conversion to gas for 5Pt1.5Ni/CNT (15.3%) was slightly higher than that of 5Pt1.5Co/CNT (14.3%) and the hydrogen gasification ratio for 5Pt1.5Ni/CNT (7.2%) was comparable to that of 5Pt1.5Co/CNT (7.7%). Noble metal Pd and Ru promoters showed different activities of glycerol conversion rate which increased to 42.58% for 5Pt2.6Ru/CNT but declined to 20.23% for 5Pt2.6Pd/CNT. Regardless the difference in glycerol conversion rate, both hydrogen gasification ratio and carbon conversion to gas for these two catalysts were promoted dramatically. In particular, the hydrogen gasification ratio for 5Pt2.6Pd/CNT (15.8%) and the carbon conversion to gas for 5Pt2.6Ru/CNT (15.1%) were 3.3 and 1.8 times higher than those of 5Pt/CNT, respectively.

### 3.2.2. Gas composition and yield

Fig. 4 demonstrates the evolution of gas product composition when metal promoters were varied. The gas products were mainly composed of $H_2$, $CO_2$, and a small amount of $CH_4$ which was less than 5%. Adding transition metals increased the $CH_4$ fraction in gas products. Hydrogen accounted for 58.9% and 53.0% over 5Pt2.7Pd/CNT and 5Pt2.6Ru/CNT, respectively. Although the catalytic activity of 5Pt1.6Cu/CNT was poor, an ultimate $H_2$ fraction of 44.4% was slightly higher than 33.2% $H_2$ of 5Pt1.5Ni/CNT and 38.4% $H_2$ of 5Pt1.5Co/CNT, which may be mainly associated with dehydrogenation of glycerol and low activity for C–C bond cleavage in reforming reaction as summarized by Wen et al. [36] and van Haasterecht et al. [8]. Wang et al. [17] has previously demonstrated that Pt-Co bimetallic catalyst supported on SWNTs was effective for hydrogen production in CAPR. In this study, 5Pt1.5Co/CNT exhibited the lowest $CH_4$ fraction (2.9%) among all Pt-based bimetallic catalysts other than moderate $H_2$ yield (177.9 $\mu$mol $min^{-1}$ $g\,cat^{-1}$).

Experimental gas production, hydrogen yield and corresponding hydrogen production rate during CAPR are summarized in Table 3. In CAPR of glycerol, the stoichiometric reforming ratio of $H_2/CO_2$ is 2.33. However, $H_2/CO_2$ ratio values in Table 3 were lower than 2.33 and the lowest $H_2/CO_2$ ratio was around 0.5 (for Pt-Ni bimetallic catalysts). This low $H_2$ concentration implied that the generated $H_2$ was consumed during hydrogenation of unsaturated intermediates. In addition, methanation in stoichiometric amounts also explained this phenomenon, leading to the formation of one $H_2$ molecule when two $CO_2$ molecules were produced [37]. Hence, $CH_4$ yield over Pt-Ni bimetallic catalysts was significantly increased by a factor of around 2.5 compared to 5Pt/CNT. In contrast, noble metals promoted Pt-based bimetallic catalysts, i.e. 5Pt2.7Pd/CNT

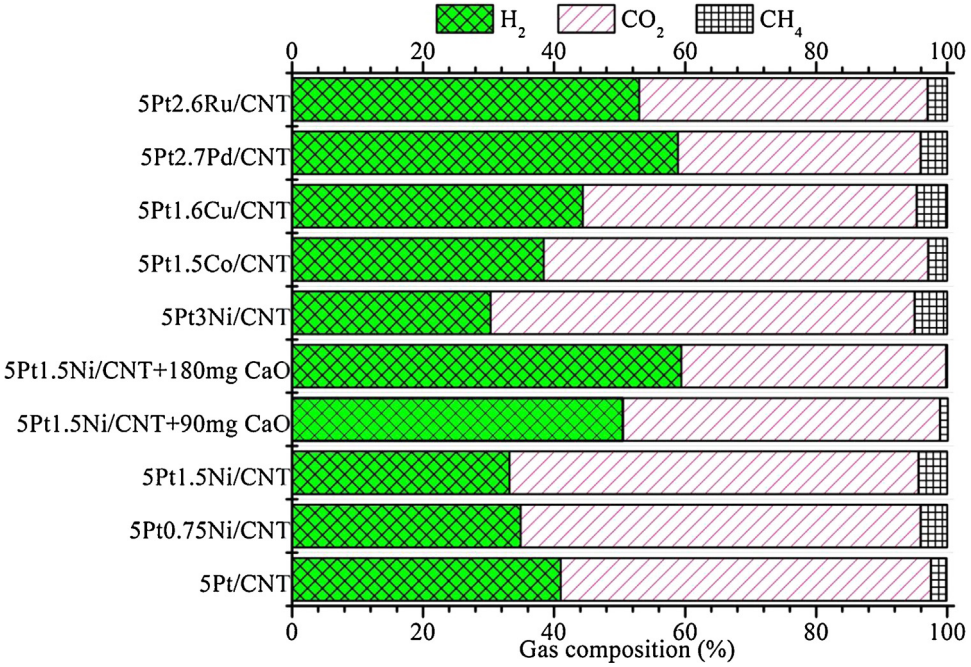


**Fig. 4.** Effects of different metal promoters and CaO amounts on gas composition during catalytic aqueous phase reforming. Operating conditions: 230 °C, an initial $N_2$ pressure of 30 bar, 15 mL of 10 wt.% glycerol with 100 mg catalyst for 4 h reaction time.

**Table 3**
Gas production and hydrogen production rate of catalytic aqueous phase reforming of glycerol.

| Catalyst | Total gas volume (mL) | $H_2$ (mL) | $CO_2$ (mL) | $CH_4$ (mL) | $H_2/CO_2$ | $H_2$ production (mmol) | $H_2$ yield (mmol/g glycerol) | $H_2$ production rate ($\mu$mol min$^{-1}$ g cat$^{-1}$) |
|---|---|---|---|---|---|---|---|---|
| 5Pt/CNT | 150.2 | 61.6 | 84.8 | 3.8 | 0.73 | 2.75 | 1.83 | 114.6 |
| 5Pt0.75Ni/CNT | 228.6 | 79.7 | 139.5 | 9.4 | 0.57 | 3.56 | 2.37 | 148.3 |
| 5Pt1.5Ni/CNT | 245.5 | 81.5 | 153.2 | 10.8 | 0.53 | 3.64 | 2.43 | 151.7 |
| 5Pt1.5Ni/CNT + 90 mg CaO | 275.8 | 139.2 | 133.4 | 3.2 | 1.04 | 6.21 | 4.14 | 258.8 |
| 5Pt1.5Ni/CNT + 180 mg CaO | 267.2 | 158.6 | 108.0 | 0.6 | 1.47 | 7.08 | 4.72 | 295.0 |
| 5Pt3Ni/CNT | 176.7 | 53.5 | 114.3 | 8.9 | 0.47 | 2.39 | 1.59 | 99.6 |
| 5Pt1.5Co/CNT | 249.0 | 95.7 | 146.0 | 7.3 | 0.66 | 4.27 | 2.85 | 177.9 |
| 5Pt1.6Cu/CNT | 83.0 | 36.8 | 42.3 | 3.9 | 0.87 | 1.64 | 1.1 | 68.3 |
| 5Pt2.7Pd/CNT | 337.5 | 198.8 | 125 | 13.7 | 1.59 | 8.88 | 5.92 | 370.0 |
| 5Pt2.6Ru/CNT | 344.8 | 182.8 | 151.7 | 10.3 | 1.21 | 8.16 | 5.44 | 340.0 |

and 5Pt2.6Ru/CNT, presented higher $H_2/CO_2$ ratio of 1.59 and 1.21, respectively. Since $CH_4$ yields over these two catalysts were comparable to that over 5Pt1.5Ni/CNT, the increased $H_2/CO_2$ ratios should be mainly attributed to disfavored hydrogenation of unsaturated intermediates.

### 3.2.3. $H_2$ and $CH_4$ selectivity

Fig. 5 represents $H_2$ and $CH_4$ selectivity in gaseous products from CAPR of glycerol over different catalysts. Compared with $H_2$ selectivity (29.8%) and $CH_4$ selectivity (4.3%) over 5Pt/CNT catalyst, all the promoters facilitated the $CH_4$ formation to different extents. Under a fixed atomic ratio (1:1) of Pt to promoter, the effect of promoters on $H_2$ selectivity was Pd > Ru > Cu > Co > Ni and that on $CH_4$ selectivity followed a descending order of Pd > Cu > Ru > Ni > Co. 5Pt2.7Pd/CNT demonstrated the highest $H_2$ selectivity (61.5%) and $CH_4$ selectivity (9.9%). $H_2$ selectivity decreased after adding Ni and Co promoters. Although $H_2$ selectivity for Pt-Ni bimetallic catalysts (18.6–23.0%) and 5Pt1.5Co/CNT (26.8%) was poor, $CH_4$ selectivity showed a high level ranging from 4.7 to 7.2% due to enhanced catalytic methanation by Co and Ni because $CH_4$ is more thermodynamically stable than $H_2$ [8].

## 3.3. Effect of Ni loading on CAPR of glycerol

In present study, the glycerol conversion rate (81.21%) and carbon conversion to gas (15.3%) over 5Pt1.5Ni/CNT were the highest among the catalysts, which might be attributed to the synergistic effects between Pt and Ni in bimetallic catalyst through Pt-Ni alloy structure formation. In addition, compared with noble metals promoted Pt-based bimetallic catalysts, 5Pt1.5Ni/CNT exhibited moderate hydrogen gasification ratio (7.2%). Thus, Pt-Ni bimetallic catalyst was selected and the effect of Ni loading was further explored. As shown in Fig. 3, glycerol conversion rate, hydrogen gasification ratio, and carbon conversion to gas for 5Pt0.75Ni/CNT were higher than 5Pt3Ni/CNT but lower than 5Pt1.5Ni/CNT. The atomic ratio (1:1) of Pt to Ni was optimal, which closely correlated with the highest activity per surface site at atomic ratio of 1:1 as Huber et al. deduced [18]. It was postulated that the excess Ni may cover the active Pt surface sites as not all the Ni formed Pt-Ni alloy [10]. Furthermore, the excess Ni which was not in Pt-Ni alloy structure would be significantly deactivated during CAPR at 225 °C [38]. When Ni loading was increased from 0.75 wt.% to 3 wt.%, $CO_2$ fraction increased gradually from 61.0% to 64.7%, while $H_2$ fraction decreased from 34.9% to 30.3%. $CH_4$ concentration remained the same. Ni was active in WGS reaction which was responsible for the improved hydrogen yield [19]. In Table 3, $H_2$ and $CO_2$ yields over 5Pt1.5Ni/CNT were remarkably higher than those over 5Pt/CNT, 5Pt0.75Ni/CNT, and 5Pt3Ni/CNT, indicating that certain amounts (i.e. 1.5 wt.%) of Ni may lead to the improvement of WGS reaction as well as excess amounts of $H_2$ production. Interestingly, as Ni loading was increased from 0.75 wt.% to 3 wt.%, $H_2$ selectivity decreased

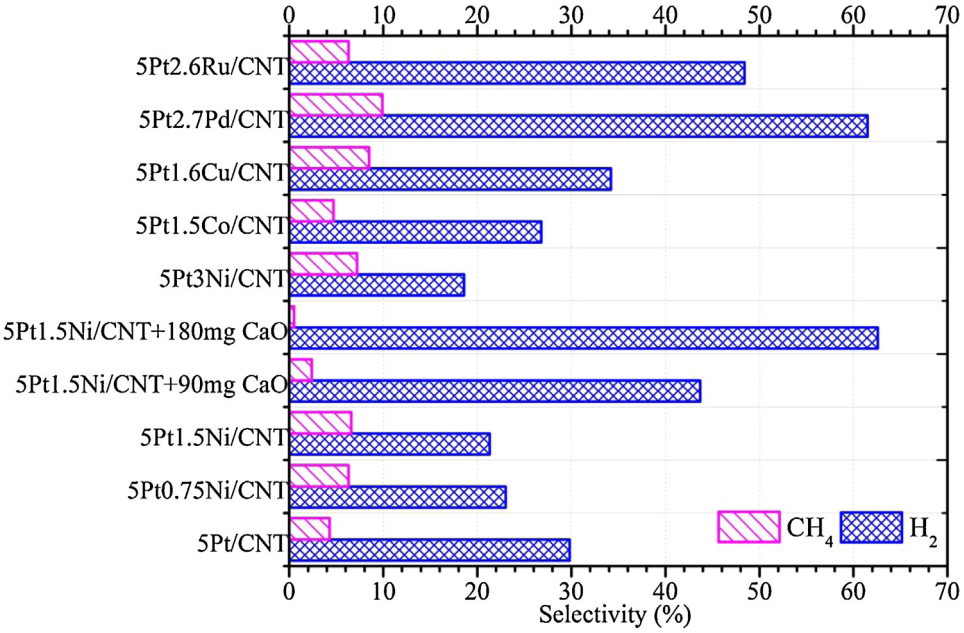


**Fig. 5.** Effects of different metal promoters and CaO amounts on $H_2$ and $CH_4$ selectivity during catalytic aqueous phase reforming. Operating conditions: 230 °C, an initial $N_2$ pressure of 30 bar, 15 mL of 10 wt.% glycerol with 100 mg catalyst for 4 h reaction time.

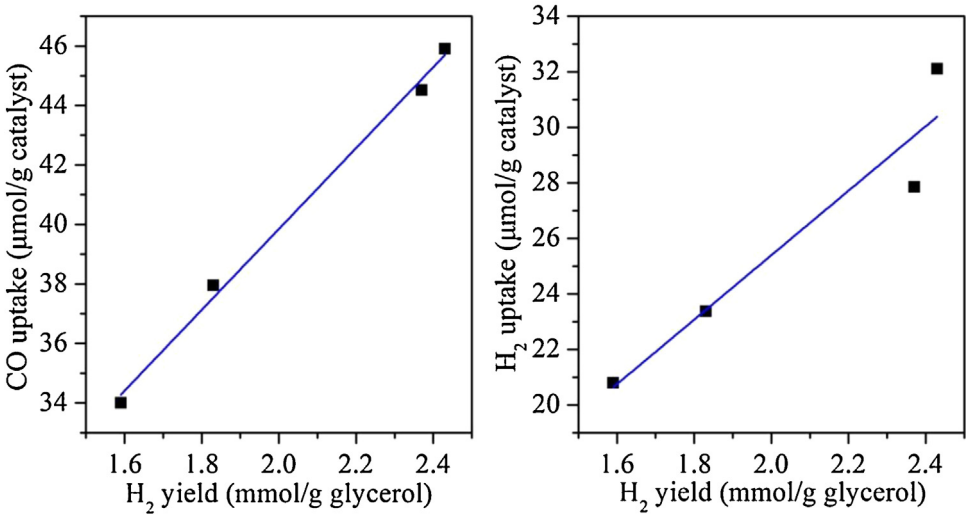


**Fig. 6.** Relationships between hydrogen yield (mmol $H_2$/g glycerol) and chemisorption uptakes (μmol/g catalyst) of $H_2$ and CO for Pt/CNT and Pt-Ni/CNT catalysts with various Pt:Ni atomic ratios.

from 23% to 18.6%, whereas $CH_4$ selectivity increased from 6.3 to 7.2%, which could be associated with the greater yield evolution of $CO_2$ than that of $H_2$ according to their definitions in Section 2.7.

According to chemisorption data shown in Table 1, $H_2$ and CO uptakes increased progressively as Ni loading was elevated to equimolar amount. However, excess Ni (Pt:Ni = 1:2) reduced $H_2$ and CO uptakes to a lower level compared to 5Pt/CNT [39]. CO uptakes were higher than $H_2$ uptakes, and the greater coverage of CO was ascribed to the stronger affinity of CO on Pt [40]. The increased uptakes of adsorbents correlated well with higher catalytic activity and $H_2$ yield. In CAPR of glycerol, CO species formed from decarbonylation of aldehyde intermediates were bound on catalyst surfaces and can interact with co-adsorbed hydrogen or $H_2O$ [41]. The increased CO uptakes promoted the reaction with $H_2O$ via WGS reaction to generate loosely bound $CO_2$ which can be readily desorbed, thereby shifting the WGS reaction towards more $H_2$ formation. Thus, lower $H_2$ yield (1.59 mmol/g glycerol) of 5Pt3Ni/CNT than that of 5Pt/CNT (1.83 mmol/g glycerol) might be due to the reduced $H_2$ and CO uptakes.

Fig. 6 illustrates the linear correlation between hydrogen yield and chemisorption uptakes of $H_2$ and CO for 5Pt/CNT and Pt-Ni/CNT catalysts with varying Pt:Ni atomic ratios. The linear regression analysis followed a previously published procedure [42]. Pearson's correlation coefficient ($R$) was employed to assess the linear correlation and the statistical significance of the correlation was analyzed using one-way analysis of variance method at a confidence level of 95% ($p < 0.05$). As displayed in Fig. 6, chemisorption uptakes of CO and $H_2$ had a remarkable positive correlation ($R = 0.998$, $p < 0.05$ and $R = 0.956$, $p < 0.05$ for CO and $H_2$, respectively) with hydrogen yield. Therefore, apart from C–C and C–O bond cleavages, adsorption capacities of $H_2$ and CO on the surface of catalysts were crucial parameters for evaluation of catalytic activity for $H_2$ production.

### 3.4. Effect of CaO addition on CAPR of glycerol

Compared with 5Pt2.7Pd/CNT and 5Pt2.6Ru/CNT, 5Pt1.5Ni/CNT exhibited the highest carbon conversion to gas (15.3%) but relatively lower hydrogen gasification ratio (7.2%). There was a great potential to improve hydrogen production at the expense of carbon conversion to gas via inhibited methanation and facilitated WGS reaction. Hence, CaO which served as sorbent was introduced to enhance WGS reaction (Eq. (2)) and reduce methanation reactions (Eqs. (3) and (4)) through $CO_2$ capture and accelerated CO removal. Different amounts (i.e. 90 mg and 180 mg) of CaO, which corresponded to Ca/(C in glycerol feedstock solution) molar ratio of 0.1 and 0.2, were attempted. With the increasing amount of CaO, the hydrogen gasification ratio was elevated from 7.2% to 11.1%, while carbon conversion to gas was reduced from 15.3% to 10.1%. The glycerol conversion rate was also increased and achieved 94.96% when a mixture of 180 mg of CaO and 100 mg of 5Pt1.5Ni/CNT was adopted. Adding CaO in the absence of catalyst did not show any catalytic activity in the same CAPR reaction. Glycerol conversion rate was only 2% along with negligible amounts of $H_2$, $CO_2$ and $CH_4$ in gas product, revealing that CaO was not active in C–C and C–H bond cleavages of oxygenated hydrocarbons under investigated hydrothermal conditions.

After adding CaO into 5Pt1.5Ni/CNT, gas composition changed dramatically. As depicted in Fig. 4, $H_2$ increased from 33.2% to 59.4%, whereas $CO_2$ decreased from 62.4% to 40.4%. The $H_2$ purity (59.4%) of 5Pt1.5Ni/CNT in the presence of 180 mg CaO was comparable to that of 5Pt2.7Pd/CNT. In addition, CaO reduced $CH_4$ to a significantly low level (0.2%). As the amount of CaO was increased to 180 mg, $H_2$ selectivity showed a pronounced increase from 21.3% to 62.6% while $CH_4$ selectivity declined from 6.6% to 0.5% over 5Pt1.5Ni/CNT catalyst. The increased $H_2$ selectivity and decreased alkane selectivity were consistent with results after adding KOH into 3%Pt-3%Re/C reported by King et al. [15].

Consequently, acting as $CO_2$ acceptor, CaO not only accelerated WGS reaction but also inhibited methanation in CAPR. Substantially low CO concentration and negligible $CH_4$ would benefit downstream application of $H_2$, e.g. proton exchange membrane fuel cells [30]. From the perspectives of $H_2$ purity and yield in CAPR reaction for renewable $H_2$ production, the combination of 5Pt1.5Ni/CNT and $CO_2$ absorber can be comparable to 5Pt2.7Pd/CNT with reduced consumption of precious metal catalyst. Moreover, it does not compromise catalyst performance.

### 3.5. Reaction pathways

Hydroxyacetone, 1,2-propanediol, ethylene glycol methanol, lactic acid, and acetic acid were detected in liquid products. Based on analyses results of gas and liquid products as well as previous research work [9,13–15,37], the plausible reaction pathways under present CAPR of glycerol for hydrogen production were primarily composed of two competitive routes, i.e. (1)

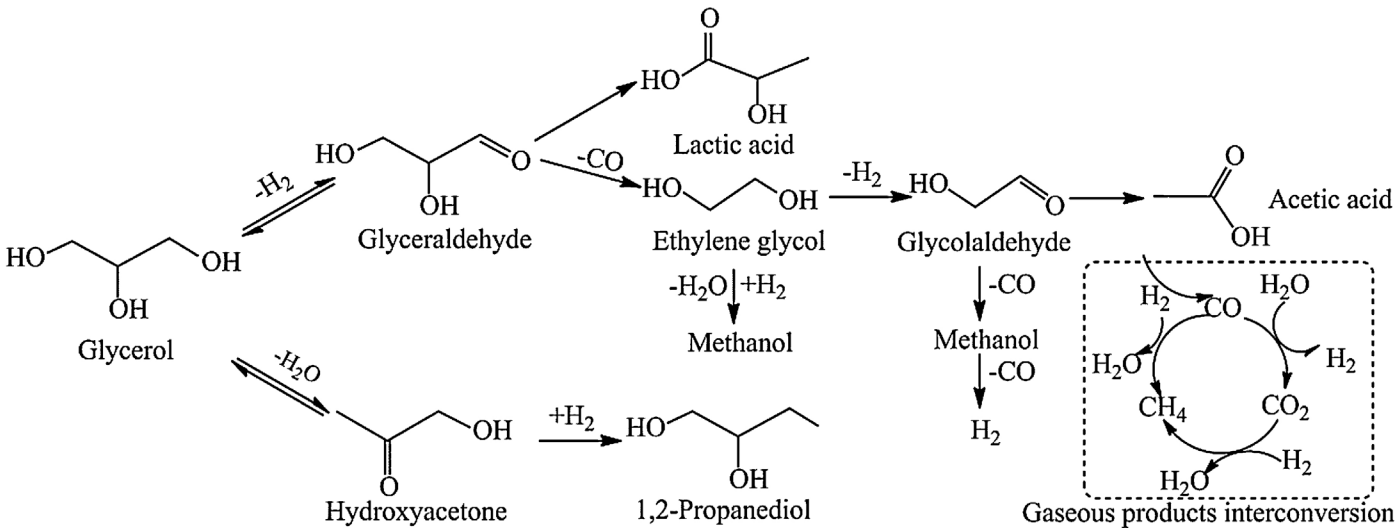


**Fig. 7.** Possible reaction pathways of catalytic aqueous phase reforming of glycerol for hydrogen production over Pt-based bimetallic catalysts supported on carbon nanotubes at 230 °C.

dehydrogenation–decarboxylation (C–C bond cleavage) and (2) dehydration–hydrogenation (C–O bond cleavage). The schematic reaction pathways are proposed in Fig. 7.

In route (1), glycerol was firstly dehydrogenated to glyceraldehyde. On one hand, glyceraldehyde went through decarbonylation to generate CO and ethylene glycol via C–C bond cleavage. As King et al. [15] reported, the dehydrogenation–decarboxylation reactions proceeded progressively to form more CO and $H_2$. CO was subsequently removed by WGS reaction to generate $H_2$ and $CO_2$. Methanol was formed via hydrogenolysis of ethylene glycol and decarbonylation of glycolaldehyde whereas acetic acid yielded from rearrangement of glycolaldehyde [8] and tended to be stable under CAPR, especially for 5Pt1.5Co/CNT (1.23 g/L). Adding promoters increased methanol formation to some extent. Specifically, methanol was increased from 12.75 to 69.04, 76.2, and 88.93 g/L over 5Pt3Ni/CNT, 5Pt2.7Pd/CNT and 5Pt2.6Ru/CNT, respectively. On the other hand, glyceraldehyde was partially converted to lactic acid. Due to effective deprotonation of glycerol and high catalytic activity of lactic acid formation from glyceraldehyde, base additives may significantly promote glycerol conversion rate and lactic acid selectivity [35]. Therefore, increased lactic acid production after adding CaO (i.e. 9.70 g/L for 180 mg CaO) may result from the basic condition. Moreover, methanol formation over 5Pt1.5Ni/CNT + 180 mg CaO (88.53 g/L) was increased by nearly 30% compared to 5Pt1.5Ni/CNT alone (68.20 g/L). The further increased methanol production was in agreement with high $H_2$ yield, which implied promoted route (1). These results may be related to the basic nature of adding CaO [24].

Dehydration rate was faster than dehydrogenation over Pt which was regarded as a solid acid [37]. In parallel route (2), glycerol was directly dehydrated to hydroxyacetone, which was a primary intermediate for the formation of 1,2-propanediol from CAPR of glycerol [14]. The hydrogenation (C–O bond cleavage) consumed $H_2$ generated from dehydrogenation (C–C bond cleavage) in route (1). Adding Ni into 5Pt/CNT decreased $H_2$ selectivity and increased $CH_4$ selectivity as shown in Fig. 5. Besides, remarkable increase of hydroxyacetone and 1,2-propanediol was also observed in Table 4. Adding Co did not show obvious difference. Compared with Pt-Ni bimetallic catalysts, far less 1,2-propanediol was formed for 5Pt1.6Cu/CNT, 5Pt2.7Pd/CNT, and 5Pt2.6Ru/CNT, suggesting that Ni can be more active for catalyzing hydrogenation of hydroxyacetone than Cu, Pd, and Ru. Interestingly, the ratio of 1,2-propanediol to hydroxyacetone for 5Pt0.75Ni/CNT and 5Pt3Ni/CNT was significantly higher than that for 5Pt1.5Ni/CNT, indicating higher hydrogenation and $H_2$ consumption. However, dramatically decreased hydroxyacetone indicated that route (2) was less favored after adding CaO. The unchanged 1,2-propanediol yield may be explained by base-catalyzed dehydration of glyceraldehyde and subsequent hydrogenation of produced pyruvaldehyde [15].

Therefore, the high glycerol conversion over Pt-Ni bimetallic catalysts was due to the promoted dehydrogenation–decarboxylation (C–C bond cleavage) in route (1) and dehydration–hydrogenation reaction in route (2). Higher $H_2$ yield for 5Pt1.5Ni/CNT was associated with lower hydrogenation rate ($H_2$ consuming) and adding CaO further favored C–C bond cleavage over 5Pt1.5Ni/CNT towards more $H_2$ yield. On

**Table 4**
Liquid products distribution after catalytic aqueous phase reforming of glycerol over different catalysts. Operating conditions: 230 °C, an initial $N_2$ pressure of 30 bar, 15 mL of 10 wt.% glycerol with 100 mg catalyst for 4 h reaction time.

| Catalyst | Concentration of liquid products (g/L) | | | | | | |
|---|---|---|---|---|---|---|---|
| | Glycerol | Hydroxyacetone | 1,2-Propanediol | Ethylene glycol | Methanol | Lactic acid | Acetic acid |
| 5Pt/CNT | 73.67 | 3.90 | 11.79 | – | 12.75 | 0.95 | 0.32 |
| 5Pt0.75Ni/CNT | 25.51 | 10.31 | 59.89 | 1.29 | 59.33 | 0.97 | 0.62 |
| 5Pt1.5Ni/CNT | 18.79 | 11.24 | 9.65 | 1.27 | 68.20 | 0.91 | 0.58 |
| 5Pt1.5Ni/CNT + 90 mg CaO | 11.12 | 0.70 | 10.17 | 1.15 | 85.00 | 7.75 | 0.40 |
| 5Pt1.5Ni/CNT + 180 mg CaO | 5.04 | 0.46 | 9.26 | 12.25 | 88.53 | 9.70 | 0.40 |
| 5Pt3Ni/CNT | 29.91 | 5.08 | 65.30 | – | 69.04 | 1.17 | 0.25 |
| 5Pt1.5Co/CNT | 24.33 | 1.78 | 13.31 | 1.09 | 14.56 | 1.77 | 1.23 |
| 5Pt1.6Cu/CNT | 86.50 | 5.93 | 0.47 | – | 30.81 | 0.26 | 0.16 |
| 5Pt2.7Pd/CNT | 79.77 | – | 2.22 | – | 76.20 | 0.14 | 0.07 |
| 5Pt2.6Ru/CNT | 57.42 | 0.17 | 4.30 | 10.61 | 88.93 | 0.23 | 0.23 |

–: Under detection limit.

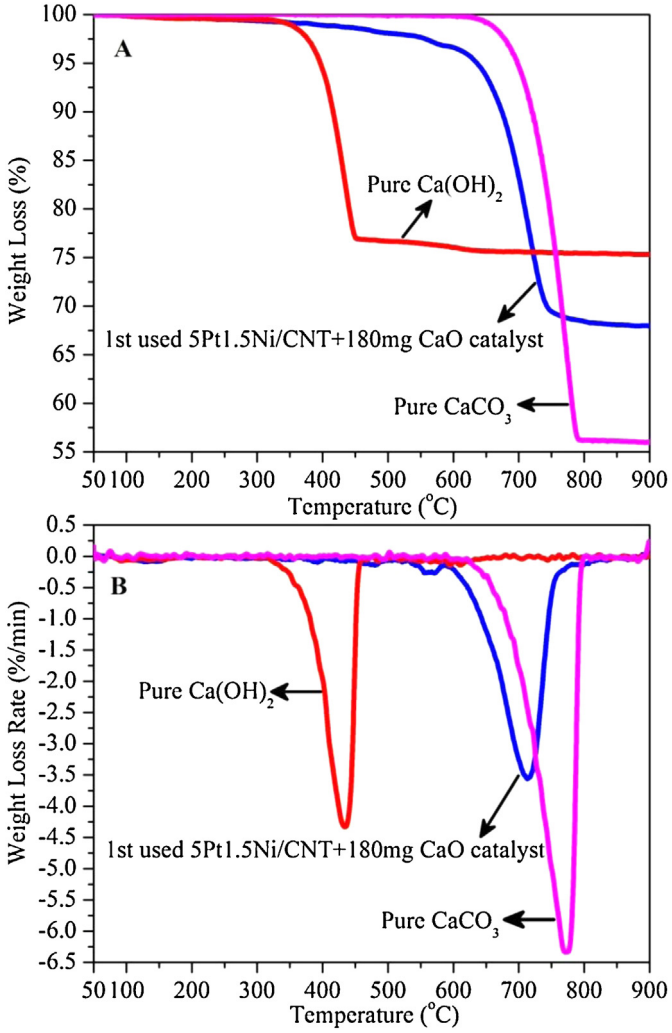


**Fig. 8.** Thermogravimetric decomposition profiles (A: TG curves; B: DTG curves) of spent 5Pt1.5Ni/CNT + 180 mg CaO catalyst, $Ca(OH)_2$ and $CaCO_3$ under $N_2$ atmosphere.

the other hand, 5Pt2.7Pd/CNT and 5Pt2.6Ru/CNT were active for dehydrogenation–decarboxylation (C–C bond cleavage) in route (1) but relatively inert to dehydration–hydrogenation (C–O bond cleavage and $H_2$ consuming) in route (2) to generate even more $H_2$ than that of combination of 5Pt1.5Ni/CNT and 180 mg CaO.

Apart from route (1) and (2), gaseous products inter-conversion contributed significantly to final gas yield and composition. The WGS reaction was a key step in CAPR of glycerol to generate more $H_2$ through reaction of removed CO with water over Pt-based catalysts [9,14]. Besides, formed $H_2$ can react with co-adsorbed CO and desorbed $CO_2$ to form $CH_4$ via methanation reactions (Eqs. (3) and (4)). As discussed in Section 3.4, CaO can inhibit $CH_4$ and facilitate WGS reaction via efficient $CO_2$ in-situ removal. King et al. [15] and Ciftci et al. [14] claimed that methane was the decomposition product of ethanol. But no distinct evidence proved that in present study. Formation pathway of methane needs further investigations.

### 3.6. Regeneration of spent catalysts and stability of recycled catalyst

Based on above discussion, combination of 5Pt1.5Ni/CNT and 180 mg CaO was identified as an effective and relatively economical catalytic system for $H_2$ production from CAPR of glycerol and thus catalytic stability of this mixture was investigated.

#### 3.6.1. Calcium distribution in CAPR of glycerol over 5Pt1.5Ni/CNT

To mitigate catalyst deactivation caused by CaO, regeneration of spent catalyst was necessary. Fig. 8 shows TG and DTG curves of pure $CaCO_3$ and $Ca(OH)_2$ as well as spent 5Pt1.5Ni/CNT + 180 mg CaO catalyst which was recovered after first catalytic run and oven drying. Different from two peaks in DTG curves reported by Onwudili and Williams [31], the DTG curve of spent catalyst showed only one peak weight loss at 712 °C which was close to 772 °C of $CaCO_3$. Upon addition of CaO into glycerol solution, $Ca(OH)_2$ will be formed. Due to the absence of peak at 432 °C for $Ca(OH)_2$, it can be inferred that $CO_2$ was excess and thus $Ca(OH)_2$ was completely converted to $CaCO_3$ as precipitant on catalyst surface. Hence, all spent catalysts were calcined at 750 °C under $N_2$ for regeneration. The residual $Ca^{2+}$ distributed in liquid products from five recycle runs was 2.16 ± 0.05 mmol, which corresponded to 121.0 ± 2.9 mg

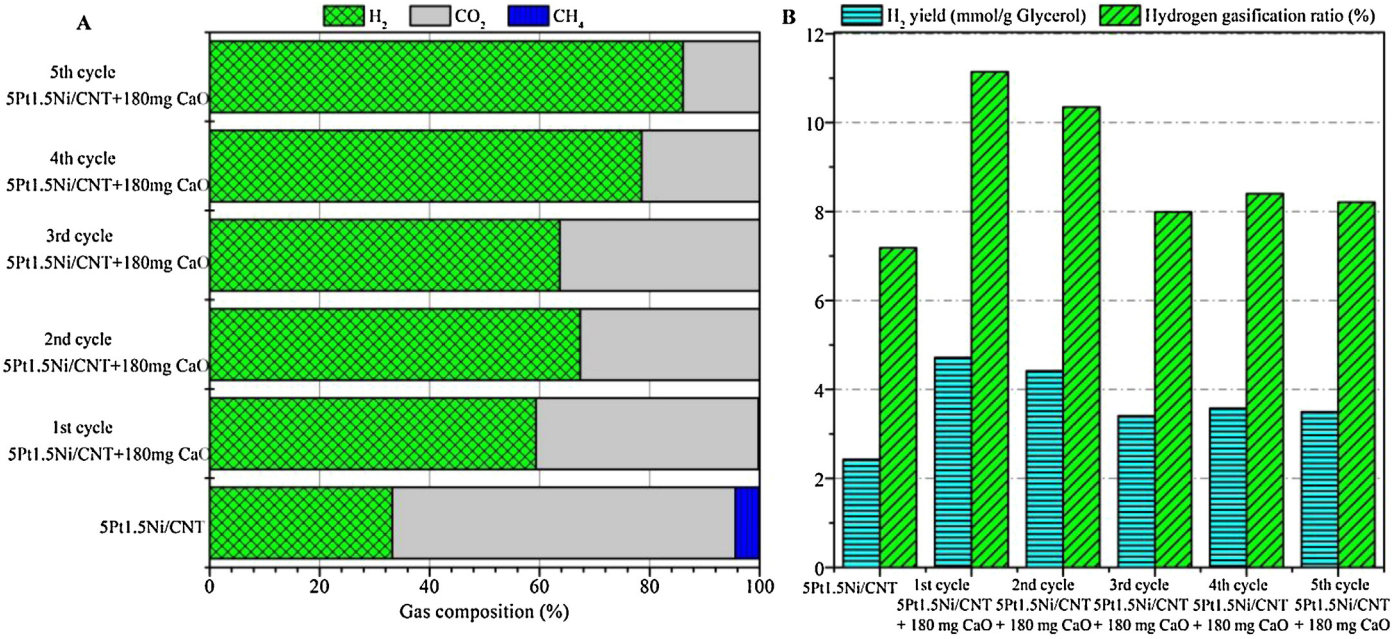


**Fig. 9.** Activity and stability of regenerated catalysts in five recycle experiments (A: gas composition; B: $H_2$ yield and hydrogen gasification ratio).

CaO. The recovered solid was around 160 mg on dry basis. Weight loss after calcination at 750 °C for 1 h was 40 mg, which was most probably in the form of $CO_2$. Thus, ca.10 wt.% (i.e. 20 mg in 180 mg) of added CaO remained in regenerated catalyst.

### 3.6.2. Catalytic performance of regenerated 5Pt1.5Ni/CNT in recycle experiments

After the spent 5Pt1.5Ni/CNT + 180 mg CaO catalyst was regenerated, 180 mg fresh CaO which served as sacrificial reagent was added in the next recycle experiment. Fig. 9 presents the catalytic performance of 5Pt1.5Ni/CNT and recycled 5Pt1.5Ni/CNT + 180 mg CaO in terms of gas composition, $H_2$ yield, and hydrogen gasification ratio. As shown in Fig. 9A, when spent 5Pt1.5Ni/CNT used in first cycle with 180 mg CaO, the fraction of $H_2$ was increased from 33.2% to 59.4% while the fraction of $CO_2$ and $CH_4$ was reduced from 62.4% and 4.4% to 40.4% and 0.21%, respectively. In the following four recycle runs, fraction of $H_2$ tended to increase to 86.1% and the fraction of $CO_2$ decreased to 13.9%. More importantly, $CH_4$ was retarded to undetectable level. This phenomenon can be related to the accumulated residual CaO after regeneration since every time fresh 180 mg CaO was introduced with spent catalyst, which accelerated $CO_2$ capture. In Fig. 9B, $H_2$ yield and hydrogen gasification ratio over 5Pt1.5Ni/CNT + 180 mg CaO slightly decreased from 4.7 mmol $H_2$/g glycerol and 11.1% in the first cycle to 3.5 mmol $H_2$/g glycerol and 8.2% in the fifth cycle, respectively. It was noted that the accumulated CaO cannot compensate the reduced 5Pt1.5Ni/CNT activity. This further confirmed CaO alone was not active in CAPR. Even though, these catalytic activities were higher than those of fresh 5Pt1.5Ni/CNT alone which demonstrated 2.4 mmol $H_2$/g glycerol and 7.2% hydrogen gasification ratio. Therefore, 5Pt1.5Ni/CNT + 180 mg CaO was an effective and stable candidate for $H_2$ rich fuel gas production from CAPR of glycerol.

## 4. Conclusions

Multi-walled carbon nanotubes supported Pt and Pt-based bimetallic catalysts have been investigated for $H_2$ production using catalytic aqueous phase reforming of glycerol. It was found that hydrogen gasification ratio and carbon conversion to gas were significantly enhanced after promoting the Pt catalyst with transition metals. Despite moderate hydrogen gasification ratio (7.2%), nickel promoted Pt catalyst (5P1.5Ni/CNT) showed the highest glycerol conversion rate (81.21%) and carbon conversion to gas (15.3%). In-situ $CO_2$ removal by adding CaO facilitated water-gas shift reaction and inhibited methanation at the expense of carbon conversion to gas. The combination of 5Pt1.5Ni/CNT and CaO decreased $CH_4$ fraction and selectivity to 0.2% and 0.5%, respectively, while $H_2$ fraction and selectivity were increased to 59.4% and 62.6%, respectively. Reaction pathways were proposed based on the results, and it showed that the improved dehydrogenation–decarboxylation and dehydration–hydrogenation reactions led to high glycerol conversion over Pt-Ni bimetallic catalysts, and a relatively low hydrogenation rate. Moreover, the introduced CaO further facilitated C–C bond cleavage over 5Pt1.5Ni/CNT towards high $H_2$ yield. Pt catalysts promoted by noble metals (i.e. Pd and Ru) were active in C–C bond cleavage but slightly inert in C–O bond cleavage and $H_2$ consuming, thereby generating more $H_2$ than Pt-Ni catalyst in the presence of CaO additives. The recovered 5Pt1.5Ni/CNT + 180 mg CaO catalyst showed excellent activity and hydrothermal stability after five recycle runs.

## Acknowledgements

The authors would like to acknowledge the Environment Technology Research Program (ETRP grant no. 1202-109) under National Environment Agency of Singapore and the academic research fund (AcRF) Tier2 (MOE2012-T2-2-041, ARC 5/13) under Ministry of Education, Singapore. We also thank Dr. Ke Yin for providing the multi-walled carbon nanotubes in catalysts preparation.

## References

[1] T.M. Mata, A.A. Martins, N.S. Caetano, Renew. Sust. Energy Rev. 14 (2010) 217–232.
[2] A.J. Byrd, K.K. Pant, R.B. Gupta, Fuel 87 (2008) 2956–2960.
[3] E. Markočič, B. Kramberger, J.G. van Bennekom, H. Jan Heeres, J. Vos, Ž. Knez, Renew. Sust. Energy Rev. 23 (2013) 40–48.
[4] A.G. Chakinala, W.P.M. van Swaaij, S.R.A. Kersten, D. de Vlieger, K. Seshan, D.W.F. Brilman, Ind. Eng. Chem. Res. 52 (2013) 5302–5312.
[5] N.H. Tran, G.S.K. Kannangara, Chem. Soc. Rev. 42 (2013) 9454–9479.
[6] D.J.M. de Vlieger, B.L. Mojet, L. Lefferts, K. Seshan, J. Catal. 292 (2012) 239–245.
[7] R. Davda, J. Shabaker, G. Huber, R. Cortright, J. Dumesic, Appl. Catal. B: Environ. 56 (2005) 171–186.
[8] T. van Haasterecht, C.C.I. Ludding, K.P. de Jong, J.H. Bitter, J. Energy Chem. 22 (2013) 257–269.
[9] Y. Guo, M.U. Azmat, X. Liu, Y. Wang, G. Lu, Appl. Energy 92 (2012) 218–223.
[10] M. El Doukkali, A. Iriondo, P.L. Arias, J. Requies, I. Gandarías, L. Jalowiecki-Duhamel, F. Dumeignil, Appl. Catal. B: Environ. 125 (2012) 516–529.
[11] G.D. Wen, Y.P. Xu, Z.S. Xu, Z.J. Tian, Catal. Commun. 11 (2010) 522–526.
[12] R.D. Cortright, R.R. Davda, J.A. Dumesic, Nature 418 (2002) 964–967.
[13] A. Ciftci, B.X. Peng, A. Jentys, J.A. Lercher, E.J.M. Hensen, Appl. Catal. A: Gen. 431 (2012) 113–119.
[14] A. Ciftci, D.A.J.M. Ligthart, E.J.M. Hensen, Green Chem. 16 (2014) 853–863.
[15] D.L. King, L. Zhang, G. Xia, A.M. Karim, D.J. Heldebrant, X. Wang, T. Peterson, Y. Wang, Appl. Catal. B: Environ. 99 (2010) 206–213.
[16] E.L. Kunkes, D.A. Simonetti, J.A. Dumesic, W.D. Pyrz, L.E. Murillo, J.G. Chen, D.J. Buttrey, J. Catal. 260 (2008) 164–177.
[17] X.M. Wang, N. Li, Z.T. Zhang, C. Wang, L.D. Pfefferle, G.L. Haller, ACS Catal. 2 (2012) 1480–1486.
[18] G.W. Huber, J.W. Shabaker, S.T. Evans, J.A. Dumesic, Appl. Catal. B: Environ. 62 (2006) 226–235.
[19] D.J.M. de Vlieger, A.G. Chakinala, L. Lefferts, S.R.A. Kersten, K. Seshan, D.W.F. Brilman, Appl. Catal. B: Environ. 111–112 (2012) 536–544.
[20] S.A. Tupy, J.G.G. Chen, D.G. Vlachos, Top. Catal. 56 (2013) 1644–1650.
[21] P.V. Tuza, R.L. Manfro, N.F.P. Ribeiro, M.M.V.M. Souza, Renew. Energy 50 (2013) 408–414.
[22] K. Koichumanova, A.K.K. Vikla, D.J.M. de Vlieger, K. Seshan, B.L. Mojet, L. Lefferts, ChemSusChem 6 (2013) 1717–1723.
[23] K. Lehnert, P. Claus, Catal. Commun. 9 (2008) 2543–2546.
[24] A.O. Menezes, M.T. Rodrigues, A. Zimmaro, L.E.P. Borges, M.A. Fraga, Renew. Energy 36 (2011) 595–599.
[25] M.M. Rahman, T.L. Church, A.I. Minett, A.T. Harris, ChemSusChem 6 (2013) 1006–1013.
[26] T.-W. Kim, H.-D. Kim, K.-E. Jeong, H.-J. Chae, S.-Y. Jeong, C.-H. Lee, C.-U. Kim, Green Chem. 13 (2011) 1718–1728.
[27] H.D. Kim, H.J. Park, T.W. Kim, K.E. Jeong, H.J. Chae, S.Y. Jeong, C.H. Lee, C.U. Kim, Catal. Today 185 (2012) 73–80.
[28] P. Azadi, R. Farnood, E. Meier, J. Phys. Chem. A 114 (2009) 3962–3968.
[29] D.J.M. de Vlieger, D.B. Thakur, L. Lefferts, K. Seshan, ChemCatChem 4 (2012) 2068–2074.
[30] J. Fermoso, F. Rubiera, D. Chen, Energy Environ. Sci. 5 (2012) 6358–6367.
[31] J.A. Onwudili, P.T. Williams, Appl. Catal. B: Environ. 132–133 (2013) 70–79.
[32] Z. Guo, Y. Chen, L. Li, X. Wang, G.L. Haller, Y. Yang, J. Catal. 276 (2010) 314–326.
[33] A.B.A.A. Nassr, I. Sinev, W. Grünert, M. Bron, Appl. Catal. B: Environ. 142–143 (2013) 849–860.
[34] H. Lin, X. Zheng, Z. He, J. Zheng, X. Duan, Y. Yuan, Appl. Catal. A: Gen. 445–446 (2012) 287–296.
[35] R.K.P. Purushothaman, J. van Haveren, D.S. van Es, I. Melián-Cabrera, J.D. Meeldijk, H.J. Heeres, Appl. Catal. B: Environ. 147 (2014) 92–100.
[36] G. Wen, Y. Xu, H. Ma, Z. Xu, Z. Tian, Int. J. Hydrogen Energy 33 (2008) 6657–6666.
[37] A. Wawrzetz, B. Peng, A. Hrabar, A. Jentys, A.A. Lemonidou, J.A. Lercher, J. Catal. 269 (2010) 411–420.
[38] R.R. Davda, J.W. Shabaker, G.W. Huber, R.D. Cortright, J.A. Dumesic, Appl. Catal. B: Environ. 43 (2003) 13–26.
[39] D.A. Simonetti, E.L. Kunkes, J.A. Dumesic, J. Catal. 247 (2007) 298–306.
[40] R. He, R.R. Davda, J.A. Dumesic, J. Phys. Chem. B 109 (2005) 2810–2820.
[41] J.R. Copeland, G.S. Foo, L.A. Harrison, C. Sievers, Catal. Today 205 (2013) 49–59.
[42] C. He, C.-L. Chen, Z. Xu, J.-Y. Wang, Environ. Technol. 35 (2013) 95–103.